Wireless coils based on resonant and nonresonant coupled-wire structure for small animal multinuclear imaging

Tania Vergara Gomez, Marc Dubois, Stanislav Glybovski, Benoit Larrat, Julien de Rosny, Carsten Rockstuhl, Monique Bernard, Redha Abdeddaim, Stefan Enoch, Frank Kober

▶ **To cite this version:**

Tania Vergara Gomez, Marc Dubois, Stanislav Glybovski, Benoit Larrat, Julien de Rosny, et al.. Wireless coils based on resonant and nonresonant coupled-wire structure for small animal multinuclear imaging. NMR in Biomedicine, 2019, 32 (5), pp.e4079. 10.1002/nbm.4079 . cea-02043238

HAL Id: cea-02043238
https://cea.hal.science/cea-02043238

Submitted on 20 Feb 2019

HAL is a multi-disciplinary open access archive for the deposit and dissemination of scientific research documents, whether they are published or not. The documents may come from teaching and research institutions in France or abroad, or from public or private research centers.

L'archive ouverte pluridisciplinaire **HAL**, est destinée au dépôt et à la diffusion de documents scientifiques de niveau recherche, publiés ou non, émanant des établissements d'enseignement et de recherche français ou étrangers, des laboratoires publics ou privés.

NMR in Biomedicine

Resonant and non-resonant wireless coils based on coupled-wire structure for small-animal multinuclear imaging

Journal:	*NMR in Biomedicine*
Manuscript ID	Draft
Wiley - Manuscript type:	Research Article
Date Submitted by the Author:	n/a
Complete List of Authors:	Vergara Gomez, Tania; Aix Marseille Univ, CNRS, Centrale Marseille, Institut Fresnel; Aix Marseille Univ, CNRS, CRMBM Dubois, Marc; Aix Marseille Univ, CNRS, Centrale Marseille, Institut Fresnel Glybovski, Stanislav; ITMO University, Department of Nanophotonics and Metamaterials Larrat, Benoit; Commissariat à l'Energie Atomique et aux Energies Alternatives, Direction de la recherche Fondamentale, NeuroSpin, Université Paris Saclay de Rosny, Julien; ESPCI Paris, PSL Research University, CNRS, Institut Langevin Rockstuhl, Carsten; Institute of Theoretical Solid State Physics, Karlsruhe Institute of Technology; Institute of Nanotechnology, Karlsruhe Institute of Technology Bernard, Monique; Aix Marseille Univ, CNRS, CRMBM Abdeddaim, Redha; Aix Marseille Univ, CNRS, Centrale Marseille, Institut Fresnel Enoch, Stefan; Aix Marseille Univ, CNRS, Centrale Marseille, Institut Fresnel Kober, Frank; Aix Marseille Univ, CNRS, CRMBM
Keywords:	RF receive coils < MR Engineering < Methods and Engineering, Computational electromagnetics < MR Engineering < Methods and Engineering, Other nuclei < MR Spectroscopy (MRS) and Spectroscopic Imaging (MRSI) Methods < Methods and Engineering, Quantitation < Post-acquisition Processing < Methods and Engineering, Body < Applications, RF transmit coils < MR Engineering < Methods and Engineering

SCHOLARONE™
Manuscripts

RESONANT AND NON-RESONANT WIRELESS COILS BASED ON COUPLED-WIRE STRUCTURE FOR SMALL-ANIMAL MULTINUCLEAR IMAGING

Tania S. Vergara Gomez[1,2], Marc Dubois[1], Stanislav Glybovski[3], Benoît Larrat[4], Julien de Rosny[5], Carsten Rockstuhl[6,7], Monique Bernard[2], Redha Abdeddaim[1*], Stefan Enoch[1], Frank Kober[2]

[1]Aix Marseille Univ, CNRS, Centrale Marseille, Institut Fresnel, 13013 Marseille, France

[2]Aix Marseille Univ, CNRS, CRMBM, Marseille, France

[3]Department of Nanophotonics and Metamaterials, ITMO University, 197101 St. Petersburg, Russia

[4]Commissariat à l'Energie Atomique et aux Energies Alternatives, Direction de la recherche Fondamentale, NeuroSpin, Université Paris Saclay, 91191 Gif-sur-Yvette, France

[5]ESPCI Paris, PSL Research University, CNRS, Institut Langevin, 75005 Paris, France

[6]Institute of Theoretical Solid State Physics, Karlsruhe Institute of Technology, 76131 Karlsruhe, Germany

[7]Institute of Nanotechnology, Karlsruhe Institute of Technology, 76021 Karlsruhe, Germany

CORRESPONDING AUTHOR

Redha Abdeddaim

Institut Fresnel

Aix Marseille Université

13013 Marseille, France

Email redha.abdeddaim@fresnel.fr

FUNDING

European Union's Horizon 2020 Research and Innovation programme under Grant Agreement No 736937, France Life Imaging National Programme grant ANR-11-INBS-0006 and the Ministry of Education and Science of the Russian Federation (project No. 14.587.21.0041 with the unique identifier RFMEFI58717X0041).

WORD COUNT: 4202

Peer Review Only

RESONANT AND NON-RESONANT WIRELESS COILS BASED ON COUPLED-WIRE STRUCTURE FOR SMALL-ANIMAL MULTINUCLEAR IMAGING

ABSTRACT

Earlier work on radiofrequency (RF) metasurfaces for preclinical MRI has targeted applications such as whole-body imaging and dual-frequency coils. In these studies, a non-resonant surface coil was used to induce currents into a metasurface that was operated as a passive inductively powered resonator. As we show in this study, the strategy of using a resonant metasurface, however, reduces the impact of the surface coil on the global performance of the whole coil. To mitigate this deficiency, we developed a new approach that relies on the combination of a commercial surface coil coupled to a non-resonant coupled-wire structure. A wireless coil based on two parallel coupled-wire structure was designed and electromagnetic field simulations were carried out with different levels of matching and coupling between both components of the coil. For experimental characterization, a prototype was built and tested at two frequencies, 300 MHz for ^{1}H and 282.6 MHz for ^{19}F at 7 T. Phantom and in vivo MRI experiments were done in different configurations to study signal and noise figures of the structure. The results showed that the proposed strategy improves the overall sensitive volume while simultaneously maintaining a high signal-to-noise ratio (SNR). Metasurfaces based on coupled wires are therefore shown here as promising and versatile elements in the MRI RF chain, as they allow customized adjustment of the sensitive volume as a function of SNR yield. In addition, they can be easily adapted to different Larmor frequencies without loss of performance.

KEYWORDS

Metasurface, RF coils, ^{19}F MRI, computational electromagnetics, whole-body imaging, metamaterials

ABBREVIATIONS

SNR: signal to noise ratio

VNA: vector network analyzer

FOV: field of view

NA: number of averages

FLASH: fast low-angle shot

RARE: rapid imaging with refocused echoes

Peer Review Only

INTRODUCTION

In clinical and preclinical magnetic resonance imaging (MRI), the commonly used radiofrequency (RF) coils belong to one out of two categories: volume and surface coils.

Volume coils such as birdcage coils [1, 2] provide uniform B_1 magnetic field in large volumes. However, when a birdcage is used for both transmission and reception of the RF field, it provides relatively low sensitivity and therefore poor SNR [3] due to generally suboptimal volume filling.

On the other hand, small surface coils usually implemented as flat copper loops, due to their superior sensitivity, can provide high SNR [4], but with the main drawback that the B_1 magnetic field decays in depth as $1/\sqrt{R^2+d^2}$, where R is the radius of the loop and d is the distance from the loop plane [5]. Consequently, the high efficiency of small surface coils is only available in a small area close to the coil. The currently most effective and established solution is the use of surface coil arrays to extend the in-plane coverage while keeping high SNR [6]. However, surface arrays are costlier, require multi-channel drivers and they are in most cases only used for signal reception. They also require specific element-wise signal recombination procedures [7], which are not trivial when phase-sensitive information is to be kept in the final image or spectrum. Finally, phased arrays are also more complicated to use for RF transmission, especially for localized spectroscopy [8].

Recently, metamaterial-inspired RF coils have been developed to bring more flexibility into the design of MRI coils for preclinical imaging. First, a volume coil based on hybridized wires has been proposed [9]. Later on, metasurfaces based on a parallel array of inductively coupled wires were explored. These wire arrays also rely on the hybridization mechanism [10] in order to obtain a homogeneous B_1 magnetic field. To do so, the wires used need to be either of a resonant length [10] or miniaturized by high-permittivity loading [11], or by capacitive interconnections [12]. These studies demonstrated the possibility of using such metasurface structures to achieve a dual-frequency coil for proton and fluorine imaging [13] and a coil for whole-body imaging with higher SNR than a volume coil [14].

It has been shown that the optimal impedance matching of such metasurface-based coils is obtained with a non-resonant feed loop when one of the metasurface resonances coincides with the targeted Larmor frequency. This configuration offers the best compromise between SNR and large sensitive volume [14]. However, the highest local SNR was still obtained with a small matched loop coil [5]. The objective of this work was to explore whether advantages can be obtained by combining both strategies. Due to mutual coupling, however, the simple combination of a resonant metasurface with a small matched loop would lead to shift of both resonances away from the original frequency [15], and a

Peer Review Only

new approach had to be developed. To assess the mutual coupling issue, we simulated the current amplitude and phase in both the loop and the coupled-wire structure.

For this purpose, we designed, simulated and built an elementary structure with two parallel wires of the same length [16]. This is indeed the minimum number of wires allowing to excite a mode with currents flowing in opposite directions in the wires. This mode behaves similarly to a long loop and allows a large coverage in the plane of the structure. The structure was studied numerically and experimentally on a 7 T preclinical scanner to verify its potential advantages over existing solutions. Namely, we hypothesized that beyond their use in a resonant regime, coupled-wire structures can be used off resonance and can be combined with a commercial surface coil instead of a non-resonant feed loop to achieve a significant improvement of sensitive volume while maintaining a high efficiency over the surface coil area. We further explored feasibility of ^{19}F MRI with the same structure on a phantom and in mice *in vivo*.

MATERIALS AND METHODS

Numerical Study

Three configurations were numerically studied (Figure 1) using CST Microwave Studio 2017 (Computer Simulation Technology GmbH, Darmstadt, Germany): (case A) a surface coil tuned and matched with lumped capacitors, (case B) a resonant coupled-wire coil with two wires of length L_0 coupled to a non-matched feed loop and (case C) a detuned coupled-wire coil with variable wire length L combined with a matched loop.

All results were obtained at a frequency of 300 MHz (Larmor frequency of ^{1}H at 7 T). In all cases, the loop had a diameter of 3 cm, and the input power used was 0.5 W. In the coupled-wire based coils, the wires were 3 cm apart, parallel to the MRI bore axis, and the loop used was placed above the wires at a distance of 1 mm and centered at the median position of the wire length. The material used for wires and loop was copper. Simulations were carried out without phantom and without RF shield.

In the first case (Figure 1A), tuning and matching of the surface coil was achieved with a matching network. For the second case (Figure 1B), impedance matching was obtained by modifying the distance between the loop and the wire plane. The resonance of the coupled-wire structure was tuned to 300 MHz by adjusting the wire length to L_0, close to a half wavelength (≈50 cm). The last case (Figure 1C) required both surface coil and coupled-wires to be detuned from the Larmor frequency to correctly tune the whole coil structure. Different wire lengths were considered, while keeping $L < L_0$ to preserve the coupled-wires in a non-resonant regime. For each length, the capacitor values of the surface coil's

Peer Review Only

matching circuit were adapted to reach impedance matching at the Larmor frequency. The current was simulated in all cases as a function of wire length (Figure 1D). Finally, the spatial B_1 amplitude profile was obtained for each case along the vertical axis in the center of the structure (Figure 1E) and along the wire length at 1 cm above them (Figure 1F).

To optimize the wire length and separation as well as analyzing the reflection coefficient (|S11|) for both frequencies (Figure 3), further simulations were carried out in the presence of a homogeneous phantom of 35x35x70 mm^3 with a relative dielectric permittivity (ε) of 76 and a conductivity (tan δ) of 0.98 S/m. The RF shield was simulated using a copper tube with 1000 mm length and 100 mm internal diameter.

Coils setups

Three different coils setups were compared as single channel transmit-receive antenna for proton and fluorine imaging: (case A) a 30 mm diameter surface coil (Bruker ^{1}H-^{19}F, model 1P T957 8V), (case B) the resonant coupled-wire coil and (case C) the non-resonant coupled-wire coil. A 70 mm diameter commercial ^{1}H birdcage coil (Bruker Biospin) was included in the tests as an additional reference, but only allowed proton imaging.

A prototype of the simulated coupled-wire structure was built using two telescopic brass tubes [17]. The wires were separated by 3 cm and placed on a plastic board of 2 mm thickness as shown in Figure 2D. Their length (L) was adjustable to tune the resonance to the desired frequency. Both wires had the same length at the end of each tuning procedure.

To build the resonant coupled-wire coil (case B), an unmatched copper loop of 3 cm diameter was printed on a 0.5 mm thick FR-4 circuit board which had an ε = 4.4 and a tan δ = 0.02 S/m (Figure 2B). The loop was fed by a coaxial cable. The matching of this coil relied on the symmetry and the distance between loop and wires. Tuning for both frequencies (300 MHz for ^{1}H or 282.6 MHz for ^{19}F) was achieved by adjusting the length of the wires to L_0 at which the coupled-wires resonate at the Larmor frequency.

To reproduce the non-resonant coupled-wire coil (case C), a commercial surface coil of 3 cm diameter (Bruker ^{1}H-^{19}F, model 1P T957 8V) (Figure 2A) was used in combination with the described coupled-wire structure. Since the commercial surface coil allowed frequency-switching from ^{1}H to ^{19}F, this coil's matching circuit could be used for final tuning and matching at both frequencies. This only required an adjustment of the wire length L such that $L < L_0$ to allow the redistribution of currents in the coil structure.

On-bench measurements of the reflection coefficient were done only for the resonant coupled-wire coil (case B) using a vector network analyzer (VNA MS2036C, Anritsu, Kanagawa, Japan) to ensure proper tuning and impedance matching for both frequencies. On-bench measurement could not be performed for the other configurations as they could not be interfaced with the VNA.

Phantom experiments

Validation of the experimental coils was done using a PharmaScan 7T MR system (Bruker Biospin, Ettlingen Germany) running ParaVision 6.0.1 software. The phantom used contained a small volume fraction of 2-2-trifluoroethanol leading to a concentration of ^{19}F nuclei on the order of 100 mmol/L (Figure 2C). The phantom was placed horizontally, parallel to the MRI bore axis, on the center of the corresponding coil.

For every tested coil, a FLASH localizer sequence was used after wobble, iterative shimming and frequency adjustment. Using the coronal slice from the localizer series, the reference power was adjusted automatically (Spin Echo/stimulated echo comparison/iteration) in a slab positioned directly adjacent to the coil surface, except for the birdcage coil, for which the reference power was adjusted without volume selection.

Single slice FLASH sequences were run in the three orientations to obtain ^{1}H images of the phantom. The parameters of the sequence were: TE/TR = 2.54/500 ms, number of averages (NA) = 1, flip angle $\alpha = 60°$, slice thickness = 0.9 mm, in-plane spatial resolution = 0.7 x 0.7 mm^2 and field of view (FOV) = 9 x 9 cm^2 with a total acquisition time of 1 min 4 sec. SNR maps were obtained from the proton images using MATLAB (MathWorks, Natick, MA, USA). Noise was calculated as the standard deviation of pixel values in a region of interest (ROI) in the lower left corner of the image where residual signal is absent. The SNR maps were calculated as the ratio of each voxel signal over the noise value of the image.

After tuning to the ^{19}F frequency, a single pulse FID sequence (TR = 3000 ms, spectral bandwidth = 7 kHz, number of points = 2048, NA = 4) was used to obtain the exact resonance frequency of 2-2-trifluoroethanol (offset -21636Hz). ^{19}F images were acquired with a T_2-TurboRARE-3D sequence with effective TE = 68.22 ms, TR = 3000 ms, RARE factor = 32, NA = 1, slice thickness = 40 mm, matrix = 64 x 64 x 32 (in-plane spatial resolution = 1 x 1 mm^2), FOV = 6 x 6 cm^2 and a total acquisition time of 20 minutes. Fluorine images were processed in MATLAB (MathWorks, Natick, MA, USA) to overlay them on ^{1}H FLASH images using a transparency of 0.6, where 0 is completely transparent and 1 is opaque.

In vivo MRI experiments

In vivo validation was performed using the same coils setups. All experiments were conducted according to a protocol approved by the University's animal experimentation committee (APAFIS#10547-2017071009112930 v4). Three C57Bl6 mice (age 9 weeks) were used for this *in vivo* demonstration. Mice were anesthetized with 3% isoflurane in an induction chamber. The animals were held under anesthesia using 1.5-1.7% isoflurane in a stream of 1 L/min room air administered through a face mask. They were placed in prone position with the abdominal region in the center of the corresponding coil (Figure 2E). Great care was taken to reproduce the same position across the different coil setups tested. Post-processing of the ^{1}H and ^{19}F images was similar to the phantom study.

The 2D FLASH sequence used for proton imaging had the following parameters: TE/TR = 2.23/50 ms, NA = 8, $\alpha = 30°$, slice thickness: 0.9 mm, in-plane spatial resolution = 0.23 x 0.23 mm^2, FOV = 6 x 6 cm^2 and a total acquisition time of 2 minutes.

Despite negligible natural endogenous fluorine concentrations in the body [18], ^{19}F imaging of the mouse abdomen *in vivo* was possible by using the signal of isoflurane, used here as anesthetic. Isoflurane is indeed known to accumulate in certain lipid compartments in anesthetized animals as shown in a recent study [19]. ^{19}F imaging was done using a FLASH sequence with TE/TR = 2.23/800 ms, NA = 32, $\alpha = 90°$, slice thickness = 3.9 mm, in-plane spatial resolution = 1.8 x 1.8 x 3.9 mm^3, frequency offset = -23537 Hz, FOV = 6 x 6 cm^2 and a total acquisition time of 13 minutes.

RESULTS

Numerical study

In figure 1D, the maximum current in the loop (red curve) and in the coupled-wire structure (blue curve) are plotted. The current in the loop was taken at the feed point as its amplitude remains almost constant due to the loop's small diameter. We monitored the wire currents in the center of the wire length where the current amplitude was maximum. It can be seen that case (B), were the resonance of the coil structure was due to the coupled-wire only, featured an extremely low current in the loop, which continuously increased when moving to a configuration where there are no wires, similar to case (A). With the wires getting shorter ($L < L_0$), the resonance shifted. Note that this change was compensated for each value of L by adjusting the capacity in the matching circuit at the loop's input. Nonetheless, the maximum current in the wires decayed continuously as the wire length was reduced.

Figure 1E shows that the maximum B_1 magnitude depends mainly on the loop current, it was

Peer Review Only

maximal for case (A) and minimal for case (B). On the other hand, the horizontal extension of the FOV was linked to the current amplitude in the wires. The non-resonant behavior, case (C), shown here for a wire length of 45 cm allowed us to obtain simultaneously a large sensitivity near the loop and to still benefit from the increased B_1 extent from the wires.

Coils setups

According to the simulations with phantom and RF shield, the reflection coefficient |S11| was lower than -20 dB in all cases for both frequencies (300 MHz for ^{1}H and 282.6 MHz for ^{19}F) as shown in Figure 3.

With the VNA, it was found that the optimal length L_0 of the wires in case (B) was 48.0 cm for ^{1}H (300 MHz) and 50.5 cm for ^{19}F (282.6 MHz), which in both cases corresponds approximately to a half wavelength in air.

In cases (A) and (C), the commercial surface coil could not be directly connected to the VNA and therefore tuning could only be done in the scanner. For case (C) a wire length of 39.0 cm was used for both nuclei, ^{19}F and ^{1}H, as the limit of tuning/matching circuit capabilities of the Bruker surface coil was reached. Nevertheless, tuning and matching of the assembled coil was good enough to perform MRI experiments.

Phantom MRI experiments

Table 1 shows the reference power values (power required for reaching a flip angle of 90° with a 1 ms pulse) obtained on the scanner for each coil with the phantom located in the center of the coil (center of wires and loop aligned). As expected, the birdcage coil required higher power than the other coils (3.89 W). The surface coil required the lowest power (0.14 W). Note that in case (C) the reference power (0.22 W) was comparable to that of the surface coil alone.

SNR maps and profiles for every coil tested with the phantom are presented in Figure 4. Figures 4I-K show that there was almost a five-fold ratio in SNR between birdcage coil/case (B) and surface coil/ case (C). The color scale has been adapted for each group, and the images have been grouped in boxes of different colors, blue for low SNR and orange for high SNR. As expected, the birdcage coil produced the lowest SNR, although it was the most homogeneous in all orientations. Case (B) provided a large imaging FOV, comparable to that of the birdcage coil but around 1.5 times higher SNR in shallow coronal slice (Figure 4B). However, Figure 4J shows that the SNR gain, as expected, was only present for a shallow depth (1.5 cm). For case (C) (Figure 4 D,H), a large enhancement of the SNR of

4.5 times was encountered at the loop location compared to case (B), as predicted by the numerical analysis above. When compared to the surface coil alone, case (C) presents a reduction of SNR of 20%. However, we observed that the FOV was enlarged in the coronal-sagittal profile (Figure 4I) giving access to areas invisible with the surface coil. At the same time, the presence of the wires in case (C) yielded a much more homogeneous SNR distribution in the axial-coronal profile (Figure 4K).

^{19}F images are presented in Figure 5. We show that the coils present the same SNR distributions as for proton imaging with the only difference that the signal was much lower due to the weak concentration of ^{19}F nuclei in the phantom. Nonetheless, the figure confirms that the SNR provided by the two coupled-wire coils (cases B and C) was enough to produce a 3D ^{19}F image from a diluted phantom within 20 minutes.

In vivo MRI experiments

Figure 6 presents the results obtained for the mouse proton MRI experiments. The behavior of the different coil setups remains consistent with the previous phantom study. Like in the phantom study, we can see that the birdcage coil has low and homogeneous SNR. Case (B) yielded higher SNR near the wires than the birdcage coil. The surface coil provided the highest SNR but the smallest FOV compared with case (C). Indeed, case (C) allowed imaging of organs away from the loop thanks to the wire contribution. At the same time, the SNR values were preserved close to the loop in the center of the FOV.

For fluorine, it was found that the Larmor frequency of ^{19}F nuclei in isoflurane was 282.577 MHz. The images are shown in Figure 7. We can see that case (C) and the surface coil provided enough sensitivity to enable a clear localization of isoflurane with the given scan parameters (Figure 7B, C). For case (B), the measured signal was comparable to the noise level making the analysis more difficult with the given scan parameters (Figure 7A).

DISCUSSION

Numerical studies of the sensitivity of coupled-wire coils show that when a resonant length (case previously considered in the literature) is used (case B), the coil performance is dominated by the wires. In this case, the current in the loop is extremely low, and, consequently a low amplitude B_1 field is generated. On the contrary, the current along the wires is almost constant leading to a wide FOV [20]. This explains why B_1 remains almost constant along the wires as shown in Figure 1F. A simple approach to benefit from the loop's and the wire's maximum contributions would be to place the

Peer Review Only

resonant coupled-wire structure on top of a loop matched with lumped capacitors. However, this option would not actually work since the interaction of the two resonant parts would inevitably affect both resonances due to strong inductive coupling. This usually leads to two hybrid resonances which frequencies are shifted away from the initially targeted frequency [21]. Our results show that we were able to combine the coupled-wire and the matched loop by tuning the wires resonance away from the Larmor frequency together with a small adjustment in the surface coil's matching circuit.

Using a non-resonant coupled-wire structure with adjustable wire length coupled to a matched loop (case C), a strong increase in the loop current could be clearly observed. The main benefit is that the length of the wires can be adapted to rearrange the distribution of currents within the different parts of the coil (loop and wires). The fact that the current in the wires dropped slowly as the wire length became shorter (blue curve in Figure 1D) allowed us to benefit from both contributions (wire and loop) when using such a configuration. This benefit can be observed more clearly in the B_1 profile of case (C) with a wire length of 45.0 cm (simulation size), shown in Figure 1E and F, where a strong increase in sensitivity at the loop position can be observed, while maintaining 75 % of the sensitivity along the wires on average. This redistribution of currents has a significant impact on the sensitivity and the field of view that can be achieved by the coil. It gives the ability to adapt the coil in terms of sensitivity and accessible volume, according to the targeted MRI application. Indeed, this new configuration was able to combine the advantages of both coupled-wire based coil with large coverage and surface coils. It may become an interesting alternative to conventional MR coil designs.

In order to explore such a concept experimentally, two parallel coupled-wire structure was designed, and a prototype was built to compare the properties in resonant and non-resonant mode with those of a standard birdcage coil and a matched surface coil. For the sake of simplicity, we chose a two-wire configuration rather than multiple wires (i.e. more than 2). Indeed, two wires is the minimum number allowing to excite the surface mode with a large coverage in the plane of the structure which behaves similarly to a large loop. More than two wires produce higher-order mode which are out of the scope of the present work. The results of the experimental study demonstrate the flexibility of the coupled-wire based coils in terms of FOV and SNR. Namely, Figures 4A-B show that case (B) yielded higher SNR than the birdcage coil, although only in the first 1.5 cm depth in the normal direction from the wires plane (Figure 4J). This depth may, however, be sufficient to obtain a satisfactory whole-body image of a mouse as shown in the *in vivo* experiments.

With case (C) it was possible to achieve high SNR at the location of the loop, with only 20% loss compared with the surface coil alone. Simultaneously, we can see that the wires contributed to enlarge

the accessible volume of the surface coil by 25% in sagittal section (Figure 4I) and its SNR homogeneity in the coronal section (Figure 4K). Equivalent performances were obtained when imaging ^{19}F nuclei contained within the phantom.

The experimental results perfectly corroborate the numerical predictions from Figure 1. We demonstrated here that the coupled-wire structure can be used in both resonant and non-resonant regimes depending on the requirements of the preclinical MRI study. Moreover, the comparison of reference power shown in Table 1 directly illustrates the strong gain obtained in terms of efficacy of the coil. This is interesting for applications that have stronger RF power requirements such as sequences involving inversion [22] or labeling pulses [23]. Finally, it is also important to stress out that the noise measured in presence of the wires was almost identical for both configurations, as presented in Table 1.

To verify the consistency of results in *in vivo* situations, proton and fluorine images were acquired from the abdomen of three mice in identical configurations as those used for the phantom scans and simulations. The *in vivo* results demonstrate that the suggested coils can indeed be used for preclinical research and comply with standard equipment requirements. The enlargement of the FOV resulting from the case (C) can be better seen in the *in vivo* images than in the phantom, especially when comparing Figure 6G that shows mainly abdominal organs and Figure 6H where heart, lungs and lower abdominal regions can be clearly seen. The *in vivo* fluorine images of the two cases (Figures 7A, C) show that both were able to detect ^{19}F within the entire mouse body, whereas the surface coil is limited to ^{19}F present in the abdomen. However, due to very low SNR, localization of the signal was difficult with the case (B) (Figure 7A).

In conclusion, we showed that coupled-wire structures can be used as parts of RF coils in both resonant and non-resonant regimes. Each of these regimes led to different current amplitude distributions within the different parts of the coil. The experiments obtained on phantom and living mice confirmed the numerical predictions on the sensitivity of the coupled-wire structure. We further showed that the coupled-wire based coils provided enough SNR to obtain ^{19}F images from isoflurane accumulated in the mouse body *in vivo* with the chosen sequence parameters. The performance of the coupled-wire based coils was not affected by the Larmor frequency difference. We believe that such structures bring a new alternative to the conventional choice between volume and surface coils. The concept of combining a carefully detuned coupled-wire structure and surface coils may help in the design of future versatile RF coils for preclinical MRI. It is worth noting that using the proposed approach, a commercial surface coil can be modified by expanding the FOV and keeping almost the

Peer Review Only

same SNR in the original area. Here the expanded region followed directly the shape of the wires. Moreover, our approach could be generalized to more complex metasurface designs including larger number of wires and different geometries.

ACKNOWLEDGEMENTS

This project has received funding from the European Union's Horizon 2020 research and innovation programme under grant agreement No 736937 and from the Ministry of Education and Science of the Russian Federation (project No. 14.587.21.0041 with the unique identifier RFMEFI58717X0041). The preclinical MRI scanner was acquired with help of the France Life Imaging National Programme - grant ANR-11-INBS-0006.

Peer Review Only

REFERENCES

[1] Hayes CE, Edelstein WA, Schenck JF, Mueller OM, Eash M. An efficient, highly homogeneous radiofrequency coil for whole-body NMR imaging at 1.5 T. Journal of Magnetic Resonance (1969) 1985;63(3):622–628.

[2] Tropp J. The theory of the bird-cage resonator. Journal of Magnetic Resonance (1969) 1989;82(1):51–62.

[3] Doty FD, Entzminger G, Kulkarni J, Pamarthy K, Staab JP. Radio frequency coil technology for small-animal MRI. NMR in Biomedicine: An International Journal Devoted to the Development and Application of Magnetic Resonance *In vivo* 2007;20(3):304–325.

[4] Keltner J, Carlson J, Roos M, Wong S, Wong T, Budinger T. Electromagnetic fields of surface coil *in vivo* NMR at high frequencies. Magnetic resonance in medicine 1991;22(2):467–480.

[5] Hoult D. The NMR receiver: a description and analysis of design. Progress in Nuclear Magnetic Resonance Spectroscopy 1978;12(1):41–77.

[6] Roemer PB, Edelstein WA, Hayes CE, Souza SP, Mueller OM. The NMR phased array. Magnetic resonance in medicine 1990;16(2):192–225.

[7] Fujita H. New horizons in MR technology: RF coil designs and trends. Magnetic Resonance in Medical Sciences 2007;6(1):29–42.

[8] Ohliger MA, Sodickson DK. An introduction to coil array design for parallel MRI. NMR in Biomedicine: An International Journal Devoted to the Development and Application of Magnetic Resonance *In vivo* 2006;19(3):300–315.

[9] Jouvaud C, Abdeddaim R, Larrat B, De Rosny J. Volume coil based on hybridized resonators for magnetic resonance imaging. Applied Physics Letters 2016;108(2):023503.

Peer Review Only

[10] Dubois M, Leroi L, Raolison Z, Abdeddaim R, Antonakakis T, de Rosny J, et al. Kerker Effect in Ultrahigh-Field Magnetic Resonance Imaging. Physical Review X 2018;8(3):031083.

[11] Shchelokova AV, Slobozhanyuk AP, Melchakova IV, Glybovski SB,Webb AG, Kivshar YS, et al. Locally enhanced image quality with tunable hybrid metasurfaces. Physical Review Applied 2018;9(1):014020.

[12] Glybovski S, Shchelokova A, Kozachenko A, Slobozhanyuk A, Melchakova I, Belov P, et al. Capacitively-loaded metasurfaces and their application in magnetic resonance imaging. In: Radio and Antenna Days of the Indian Ocean (RADIO), IEEE; 2015. 1–2 p.

[13] Hurshkainen A, Nikulin A, Georget E, Larrat B, Berrahou D, Neves AL, et al. A novel metamaterial-inspired RF-coil for preclinical dual-nuclei MRI. Scientific reports 2018;8(1):9190.

[14] Zubkov M, Hurshkainen AA, Brui EA, Glybovski SB, Gulyaev MV, Anisimov NV, et al. Small-animal, whole-body imaging with metamaterial-inspired RF coil. NMRin Biomedicine 2018;31(8):e3952.

[15] l Mispelter J, Lupu M, Briguet A. NMR probeheads for biophysical and biomedical experiments: theoretical principles & practical guidelines. Imperial College Press; 2006.

[16] Glybovski SB, Tretyakov SA, Belov PA, Kivshar YS, Simovski CR. Metasurfaces: From microwaves to visible. Physics Reports 2016;634:1–72.

[17] Shchelokova AV, van den Berg CA, Dobrykh DA, Glybovski SB, Zubkov MA, Brui EA, et al. Volumetric wireless coil based on periodically coupled split-loop resonators for clinical wrist imaging. Magnetic resonance in medicine 2018;80(4):1726–1737.

[18] Ruiz-Cabello J, Barnett BP, Bottomley PA, Bulte JW. Fluorine (^{19}F) MRS and MRI in biomedicine. NMR in Biomedicine 2011;24(2):114–129.

[19] Constantinides C, Maguire ML, Stork L, Swider E, Srinivas M, Carr CA, et al. Temporal

Peer Review Only

accumulation and localization of isoflurane in the C57BL/6 mouse and assessment of its potential contamination in ^{19}F MRI with perfluoro-crown-etherlabeled cardiac progenitor cells at 9.4 Tesla. Journal of Magnetic Resonance Imaging 2017;45(6):1659–1667.

[20] Orfanidis SJ. Electromagnetic waves and antennas. Rutgers University New Brunswick, NJ; 2002.

[21] Mett RR, Sidabras JW, Hyde JS. MRI surface-coil pair with strong inductive coupling. Review of Scientific Instruments 2016;87(12):124704.

[22] Weigel M, Zaitsev M, Hennig J. Inversion recovery prepared turbo spin echo sequences with reduced SAR using smooth transitions between pseudo steady states. Magnetic resonance in medicine 2007;57(3):631–637.

[23] Alsop DC, Detre JA, Golay X, Günther M, Hendrikse J, Hernandez-Garcia L, et al. Recommended implementation of arterial spin-labeled perfusion MRI for clinical applications: A consensus of the ISMRM perfusion study group and the European consortium for ASL in dementia. Magnetic resonance in medic 2015;73(1):102–116.

Peer Review Only

TABLES

Table 1: Analysis of ^{1}H results. The table shows the reference powers obtained for the different coils after radiofrequency autocalibration of the magnet, the average standard deviation of noise calculated from both coronal and sagittal images, and the comparison of the FOV and SNR obtained from each coil.

Coil	Ref. Power (W)	Average σ	FOV and SNR
Birdcage coil	3.89	$1.55e^{-5}$	Whole-body with homogeneous and low SNR (100)
Case B	0.96	$1.35e^{-5}$	Whole-body with higher SNR (250) in shallow depth
Surface	0.14	$1.35e^{-5}$	Reduced FOV with high SNR (1200)
Case C	0.22	$1.21e^{-5}$	Wider FOV with a local SNR of (900)

Peer Review Only

FIGURE LEGENDS

Figure 1: Numerical analysis of the three configurations: Sketch of (A) surface coil with a matching circuit, (B) resonant coupled-wire coil conformed by two wires with length L_0 (49 cm) coupled with an unmatched feed loop and (C) non-resonant coupled-wire coil that combines a matched surface coil with two wires of length L smaller than the resonant length L_0. The diameter of the loop in all cases is 3 cm and the wires are 3 cm apart. (D) shows the plot of the current amplitudes in the loop (red) and in the wires (blue) with the different configurations. In each of the configurations the coil was tuned and matched to 300 MHz, and 0.5 W of input power was used. (E) shows the B_1 profiles obtained along a vertical line through the center of the coil and (F) is the B_1 evaluated on a horizontal line along the wires at 1 cm above the wire plane.

Figure 2: Coupled-wire inspired coil for 7 T small animal imaging: (A) picture of the commercial surface coil (Bruker, model 1P T957 8V); (B) picture of the printed loop of 3 cm diameter on circuit board (FR-4, 0.5 mm thickness) and fed through a coaxial cable; (C) Bruker $^{19}F/^{1}H$ phantom of 3.5x3.5x9 cm^3 used during on-bench measurements and MRI scans, concentration of ^{19}F of 100 mmol/L; (D) picture of the coupled-wire structure with 2 telescopic wires separated by 3 cm and placed on a plastic board; (E) picture of the *in vivo* experimental setup.

Figure 3: |S11| simulation and on-bench measurements for the case (B) and |S11| simulations for the surface coil and the case (C) (^{1}H and ^{19}F Larmor frequencies).

Figure 4: Coronal and sagittal SNR maps in gray scale (dash lines locate the profile cuts). (A),(E) birdcage coil; (B),(F) case B; (C),(G) surface coil; (D),(H) case C. The cyan line gives the coronal-sagittal profiles (I); the red line gives the sagittal-axial profiles (J) and the yellow line gives the axial-coronal profiles (K). Noise standard deviation is given on top of each map.

Figure 5: ^{19}F T_2-turboRARE-3D image in jet color map acquired with: (A) case B ; (B) surface coil and (C) case C in sagittal orientation. The images were overlaid on top of ^{1}H FLASH images in gray scale.

Figure 6: *In vivo* ^{1}H SNR maps. Sagittal and coronal-plane images with: (A), (E) birdcage coil; (B),

Peer Review Only

(F) case B; (C), (G) surface coil and (D), (H) case C. Low SNR images are in a blue box with a scale of 0 to 60. High SNR images are in an orange box with a scale of 0 to 130.

Figure 7: *In vivo* ^{19}F FLASH coronal-plane images in jet scale obtained with: (A) case B; (B) surface coil and (C) case C. The images were overlaid on top of ^{1}H FLASH images in gray scale.

Peer Review Only

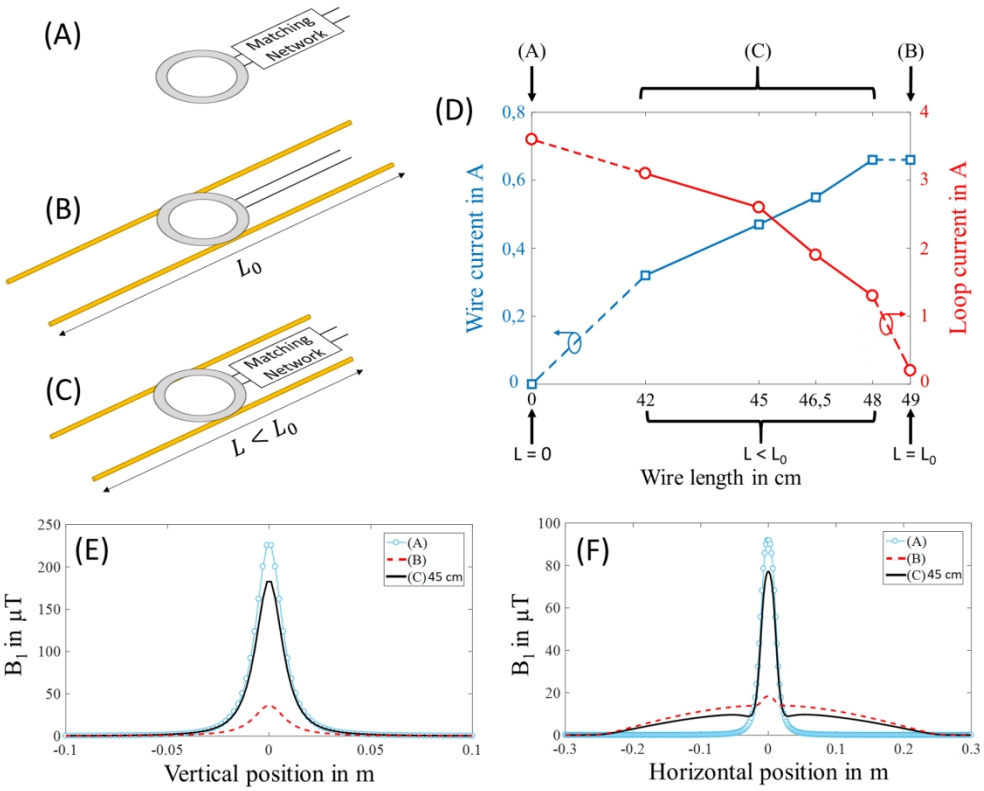

Figure 1: Numerical analysis of the three configurations: Sketch of (A) surface coil with a matching circuit, (B) resonant coupled−wire coil conformed by two wires with length L_0 (49 cm) coupled with an unmatched feed loop and (C) non−resonant coupled−wire coil that combines a matched surface coil with two wires of length L smaller than the resonant length L_0. The diameter of the loop in all cases is 3 cm and the wires are 3 cm apart. (D) shows the plot of the current amplitudes in the loop (red) and in the wires (blue) with the different configurations. In each of the configurations the coil was tuned and matched to 300 MHz, and 0.5 W of input power was used. (E) shows the B_1 profiles obtained along a vertical line through the center of the coil and (F) is the B_1 evaluated on a horizontal line along the wires at 1 cm above the wire plane.

160x126mm (300 x 300 DPI)

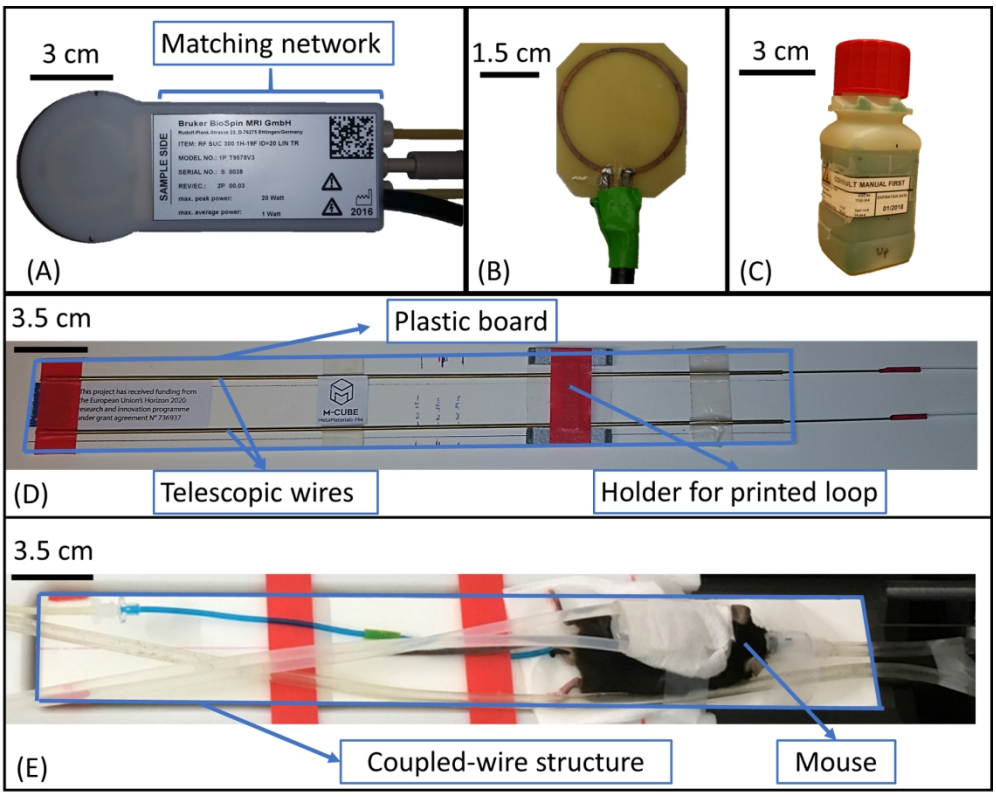

Figure 2: Coupled-wire inspired coil for 7 T small animal imaging: (A) picture of the commercial surface coil (Bruker, model 1P T957 8V); (B) picture of the printed loop of 3 cm diameter on circuit board (FR−4, 0.5 mm thickness) and fed through a coaxial cable; (C) Bruker $^{19}F/^{1}H$ phantom of 3.5x3.5x9 cm^3 used during on−bench measurements and MRI scans, concentration of ^{19}F of 100 mmol/L; (D) picture of the coupled−wire structure with 2 telescopic wires separated by 3 cm and placed on a plastic board; (E) picture of the *in vivo* experimental setup.

160x127mm (300 x 300 DPI)

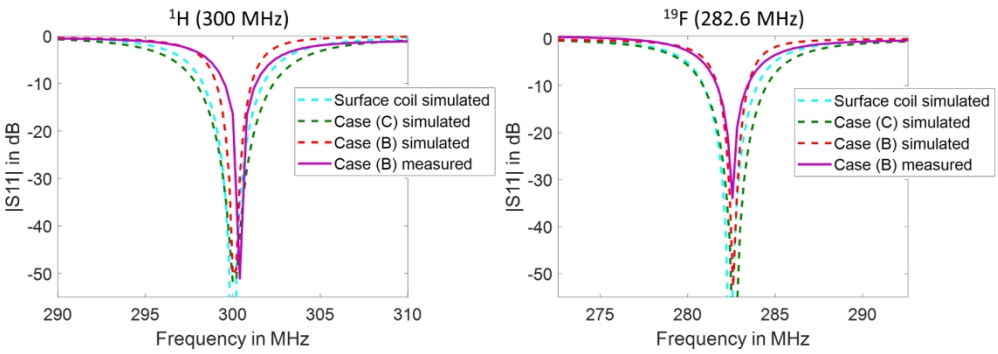

Figure 3: |S11| simulation and on-bench measurements for the case (B) and |S11|simulations for the surface coil and the case (C) (^{1}H and ^{19}F Larmor frequencies).

160x56mm (300 x 300 DPI)

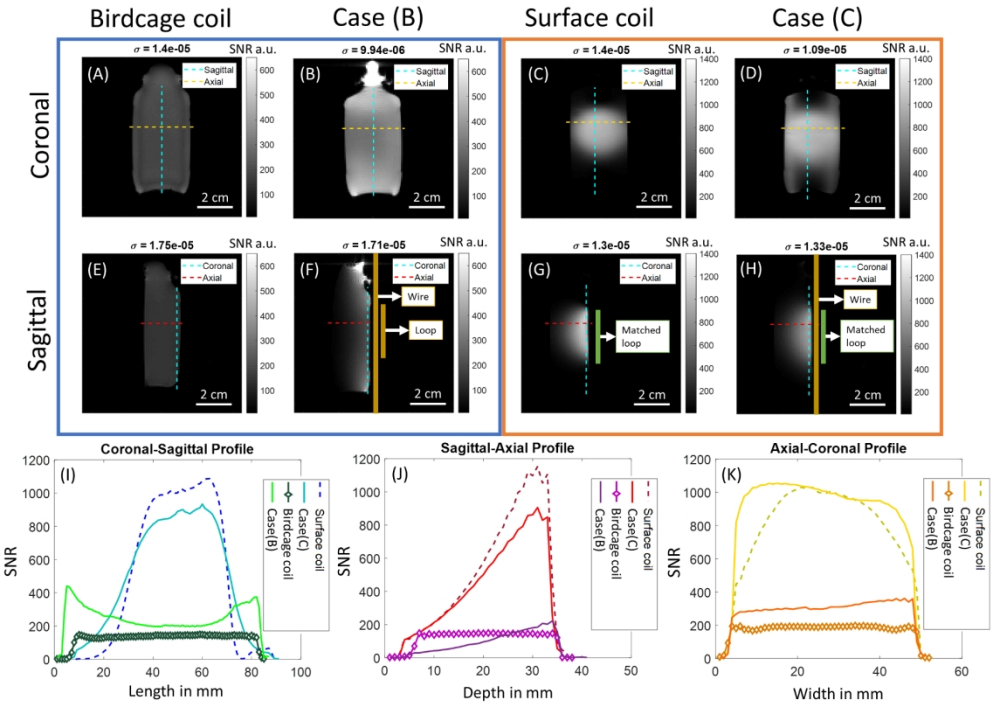

Figure 4: Coronal and sagittal SNR maps in gray scale (dash lines locate the profile cuts). (A),(E) birdcage coil; (B),(F) case B; (C),(G) surface coil; (D),(H) case C. The cyan line gives the coronal−sagittal profiles (I); the red line gives the sagittal−axial profiles (J) and the yellow line gives the axial−coronal profiles (K). Noise standard deviation is given on top of each map.

160x115mm (300 x 300 DPI)

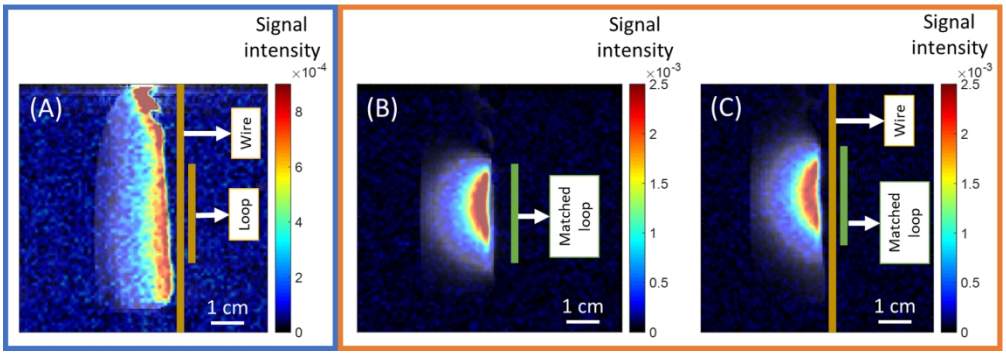

Figure 5: ^{19}F T_2-turboRARE-3D image in jet color map acquired with: (A) case B ; (B) surface coil and (C) case C in sagittal orientation. The images were overlaid on top of ^{1}H FLASH images in gray scale.

160x55mm (300 x 300 DPI)

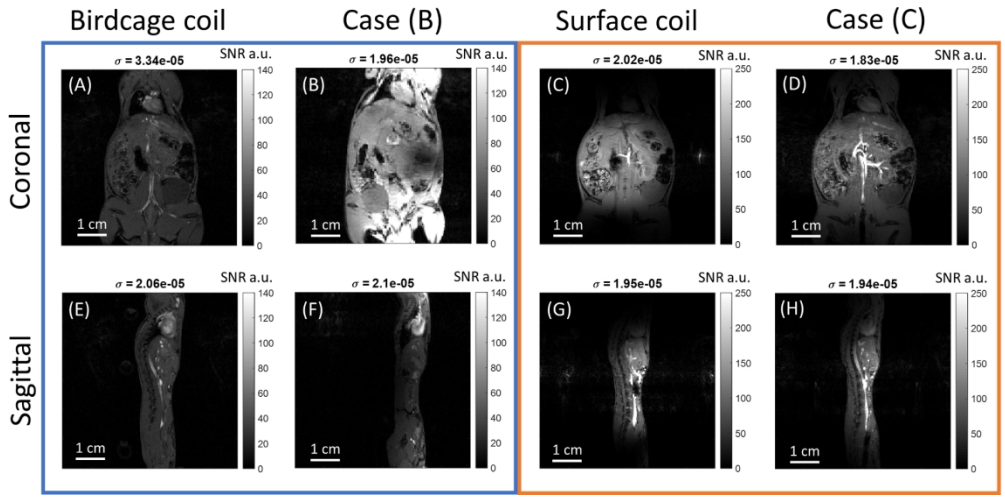

Figure 6: *In vivo* ^{1}H SNR maps. Sagittal and coronal−plane images with: (A), (E) birdcage coil; (B), (F) case B; (C), (G) surface coil and (D), (H) case C. Low SNR images are in a blue box with a scale of 0 to 60. High SNR images are in an orange box with a scale of 0 to 130.

160x78mm (300 x 300 DPI)

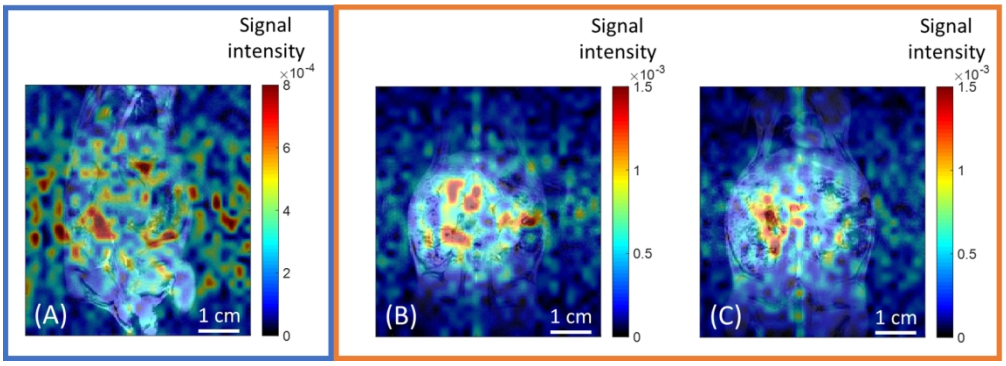

Figure 7: *In vivo* ^{19}F FLASH coronal-plane images in jet scale obtained with: (A) case B; (B) surface coil and (C) case C. The images were overlaid on top of ^{1}H FLASH images in gray scale.

160x57mm (300 x 300 DPI)

GRAPHICAL ABSTRACT

RESONANT AND NON-RESONANT WIRELESS COILS BASED ON COUPLED-WIRE STRUCTURE FOR SMALL-ANIMAL MULTINUCLEAR IMAGING

Tania S. Vergara Gomez, Marc Dubois, Stanislav Glybovski, Benoît Larrat, Julien de Rosny, Carsten Rockstuhl, Monique Bernard, Redha Abdeddaim*, Stefan Enoch, Frank Kober

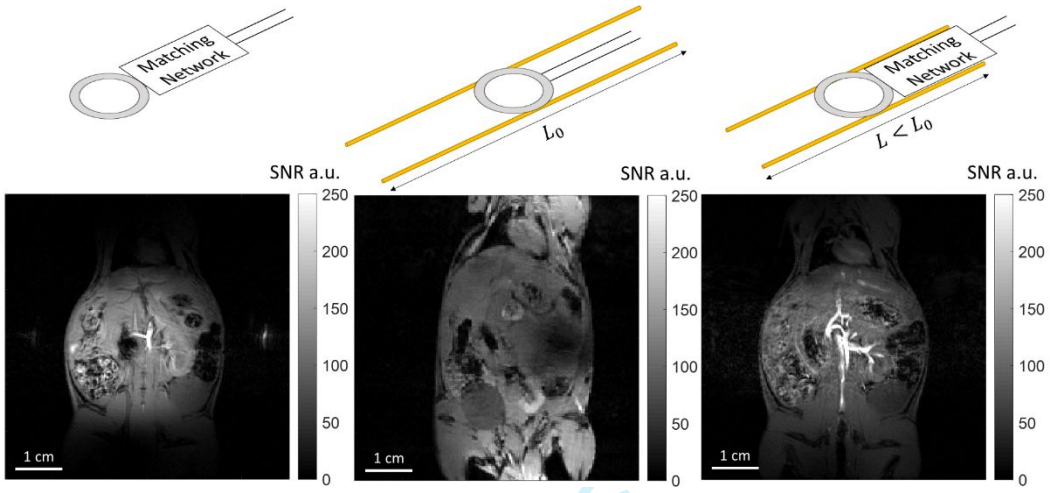

Using a resonant metasurface coil based on coupled wires reduces the impact of the coupling loop itself on the coil performance. To mitigate this, we developed a new approach that relies on the combination of a commercial surface coil and a non-resonant coupled-wire structure. This non-resonant coupled-wire coil was designed, simulated, built and tested at ^{1}H and ^{19}F at 7 T. The results showed that this new strategy improves the coil's FOV while simultaneously maintaining a high SNR.